Environmental Research 192 (2021) 110242

Contents lists available at ScienceDirect

Environmental Research

journal homepage: www.elsevier.com/locate/envres

Dramatically enhanced degradation of recalcitrant organic contaminants in MgO_2/Fe(III) Fenton-like system by organic chelating agents

Yun Bai [a], Doudou Wu [a], Wei Wang [a,*], Pei Chen [a], Fatang Tan [a], Xinyun Wang [a], Xueliang Qiao [a], Po Keung Wong [b]

[a] State Key Laboratory of Material Processing and Die & Mould Technology, Huazhong University of Science and Technology, Wuhan, 430074, Hubei, China
[b] School of Life Sciences, The Chinese University of Hong Kong, Shatin, NT, Hong Kong, China

ARTICLE INFO

Keywords:
Magnesium peroxide nanoparticle
Fenton-like reaction
Chelating agent
Hydroxyl radical
Organic contaminant

ABSTRACT

Herein, the application of organic acids as chelating agent, including citric acid (CA), tartaric acid (TA), oxalic acid (OA) and ethylenediaminetetraacetic acid (EDTA), to enhance the degradation performance of MgO_2/Fe(III) system was investigated in the terms of chelating agent dosage, Fe(III) dosage, reaction temperature, initial solution pH and inorganic anion. When the molar ratio of MgO_2/Fe(III)/chelating agent was 1 : 0.7 : 0.3, the degradation efficiencies of Rhodamine B (RhB) increased from 6.7% (without chelating agent) to 42.3%, 98.5%, 48.9% and 25.8% within 30 min for CA, TA, OA, and EDTA, respectively. The promotion effect was mainly attributed to the chelation between chelating agents and Fe(III), rather than the acidification of chelating agents. The pseudo-first-order kinetic model well fitted RhB degradation in MgO_2/Fe(III)/TA system, and the kinetic rate constant reached up to 0.295 min^{-1}. Hydroxyl radical was confirmed to be the dominant active species to degrade organics in the MgO_2/Fe(III)/TA system. Notably, the degradation system could work in a broad pH (3–11) and temperature (5–35 °C) range. Moreover, the MgO_2/Fe(III)/TA system can also effectively degrade methylene blue, tetracycline and bisphenol A. This work provided a new, efficient and environmentally-friendly Fenton-like system for stubborn contaminant treatment.

1. Introduction

Fenton/Fenton-like reaction, as one of advanced oxidation processes (AOP), is a promising strategy for efficient degradation of diverse recalcitrant contaminants due to the high oxidation capacity. Generally, the Fenton/Fenton-like reaction system consists of a catalyst and an oxidant. Transition metal compounds and their complexes are often used as homogeneous or heterogeneous catalysts (Leal et al., 2018; Ouyang et al., 2019a; Yamaguchi et al., 2018). Liquid H_2O_2 is one of the most commonly used Fenton oxidants, due to that it can be catalytically decomposed to produce lots of active species, involving peroxide ions (O_2^{2-}), hydroxyl radicals (•OH) and superoxide anions ($•O_2^-$) (Sun et al., 2020; Miklos et al., 2018; Moreira et al., 2017). However, it works effectively in a narrow pH range (2–4). Although various photo-Fenton catalysts were developed to broaden the working pH range, they suffered from tedious preparation procedures, low efficiency and external energy consumption (Miao et al., 2020; Pulgarin et al., 2020; Yue et al., 2020).

Recently, solid oxidants including metal peroxides (Liu et al., 2020a; Gholami et al., 2019; Giannakoudakis et al., 2018; Northup and Cassidy, 2008), persulfate (Bararpour et al., 2018; Wang and Wang, 2018) and percarbonate (Yu et al., 2018) have aroused great interest and attention in Fenton/Fenton-like reaction. Different from liquid H_2O_2, solid oxidants are relatively safer and more stable, which make their transportation and preservation more convenient. Besides, solid oxidants can produce active species in a wide pH range and have a continuous effect on organics degradation due to the slow release of active species from the decomposition of oxidants (Giannakoudakis et al., 2018; Wu et al., 2019). Therefore, solid oxidants are ideal substitutes for H_2O_2 as oxidants in Fenton or Fenton-like reaction system.

Since metal peroxides (CaO_2, ZnO_2 and MgO_2) possess the advantages of low cost, easy preparation and low even no toxicity, they have been widely reported for environmental purification in the last several years (Lu et al., 2019; Wolanov et al., 2013; Wu et al., 2019; Zhang et al., 2018a and Liu et al., 2020b). Their applications in Fenton-like degradation of organic pollutants will not cause secondary pollution, because

* Corresponding author.
E-mail address: weiwang@hust.edu.cn (W. Wang).

https://doi.org/10.1016/j.envres.2020.110242
Received 4 January 2020; Received in revised form 13 September 2020; Accepted 16 September 2020
Available online 26 September 2020

there are almost no other released ions (such as K^+, NH_4^+, SO_4^{2-}, CO_3^{2-}) in aqueous solution, except for the formation of metal hydroxide precipitates. Among these peroxides, MgO_2 has higher active oxygen content and more environmentally friendly characteristic (Gholami et al., 2019; Wu et al., 2019). Hence, MgO_2 used as Fenton-like oxidant has a promising prospect in the remediation of organic-contaminated water and soil. However, as an alkaline peroxide, MgO_2 can react with water to give $Mg(OH)_2$ (Eq. (1)), then partial $Mg(OH)_2$ will dissociate into OH^-, leading to a rise in solution pH. Consequently, Fe(II)/Fe(III) as catalysts in a Fenton-like system will be precipitated into iron hydroxides ($Fe(OH)_x$ or $FeO_x(OH)_y$), which will seriously restrict their catalytic performances (Miao et al., 2015; Subramanian and Madras, 2017).

$$MgO_2 + 2H_2O \rightarrow Mg(OH)_2 + H_2O_2 \quad (1)$$

In order to promote the degradation efficiency and inhibit the precipitation of Fe(II)/Fe(III) in high pH (pH > 4), various chelating agents were applied to chelate Fe(II)/Fe(III) in Fenton-like reaction system. The compounds containing coordinating groups, such as carboxyl (–COOH), hydroxyl (–OH) and amino ($–NH_2$), can chelate iron by donating a pair of electrons to Fe(II)/Fe(III) (Pignatello et al., 2006; Zhang et al., 2019). Among them, organic acids are one of the most commonly used chelating agents. In the Fe(II)/peroxymonosulfate system, protocatechuic acid could raise the degradation of ciprofloxacin in a wide pH range (3–9) (Ouyang et al., 2019b), and it could also significantly accelerate the degradation of alachlor by 10000 times at pH 3.6 (Qin et al., 2015). This enhancement was mainly ascribed to the chelating and reduction of protocatechuic ligand. It could complex with Fe(II)/Fe(III) to inhibit their precipitation and speed up the Fe(II)/Fe(III) redox couple to generate reactive oxygen species (ROS). Oxalic acid (OA) was considered to be most effective chelating agent for the simultaneous removal of various organic contaminants (benzene, toluene, ethylbenzene and xylene) in the CaO_2/Fe(II) system (Xue et al., 2018), while citric acid (CA) was a more suitable chelating agent in the Fe(II) activated persulfate system (Liang et al., 2008). It can be seen that the effect of chelating agents on different Fenton-like degradation systems is different. However, the use of chelating agents to promote the performance of MgO_2/Fe(III) system in degrading stubborn organic contaminants has not been studied until now.

Herein, CA, OA, tartaric acid (TA) and ethylenediaminetetraacetic acid (EDTA), whose chemical structures contained different amounts of –COOH and –OH (Fig. S1), were selected as chelating agents to boost the degradation capacity of MgO_2/Fe(III) system towards stubborn organic contaminants. The effect of chelating agents on the MgO_2/Fe(III) degradation system was systematically investigated as functions of chelating agent amount, Fe(III) dosage, reaction temperature, initial solution pH, different types of organic contaminant and coexisting inorganic anion. The ROS produced in the MgO_2/Fe(III)/TA system was identified through electron paramagnetic resonance (EPR) measurement and scavenger tests. Further, the concentration of total Fe ions in the reaction system was measured to confirm the chelation between chelating agents and Fe ions. Additionally, the generated precipitate after degradation reaction was reused as Fenton-like catalyst to trigger MgO_2 to degrade organic contaminants.

2. Materials and methods

2.1. Materials

Magnesium nitrate ($Mg(NO_3)_2{\cdot}6H_2O$), anhydrous ethanol (C_2H_5OH), aqueous ammonia ($NH_3{\cdot}H_2O$, 25–28 wt%), hydrogen peroxide (H_2O_2, 30 wt%), sulfuric acid (H_2SO_4, 95.0–98.0 wt%), sodium hydrogen carbonate ($NaHCO_3$), sodium nitrate ($NaNO_3$), sodium hydroxide (NaOH), citric acid (CA), ethylenediaminetetraacetic acid (EDTA), bisphenol A (BPA), p-benzoquinone (BQ) and methylene blue (MB) were obtained from Sinopharm Chemical Reagent Co., Ltd. Ferric sulfate ($Fe_2(SO_4)_3{\cdot}xH_2O$), isopropanol (IPA) and oxalic acid (OA) were purchased from Shanghai Chemical Reagent Factory. Sodium chloride (NaCl) and tartaric acid (TA) were gotten from Tianjin Chemical Reagent Factory. 5, 5-dimethyl-1-pyrroline N-oxide (DMPO), Rhodamine B (RhB) and tetracycline (TC) were supplied by Aladdin Chemistry Reagent Chemistry Co., Ltd. All chemical reagents were directly used as received without any pretreatment.

2.2. Synthesis and content analysis of MgO_2 nanoparticles

The highly pure MgO_2 sample were prepared according to the method reported in our previous work (Wu et al., 2019). The active oxygen content and purity of the prepared MgO_2 nanoparticles were quantitatively evaluated using the permanganate (0.02 M) titration methods (Giannakoudakis et al., 2018) (Eqs. (2)–(5)).

$$MgO_2 + 2H^+ \rightarrow Mg^{2+} + H_2O_2 \quad (2)$$

$$2KMnO_4 + 5H_2O_2 + 3H_2SO_4 \rightarrow K_2SO_4 + 2MnSO_4 + 5O_2\uparrow + 8H_2O \quad (3)$$

$$\text{Active oxygen content: } [O] = \frac{80 \times V \times C}{m} \times 100\% \quad (4)$$

$$\text{Purity: } MgO_2\% = \frac{[O]}{28.57} \times 100\% \quad (5)$$

Where C and V are the concentration (mol/L) and consumed volume (L) of $KMnO_4$ in the titration experiment, and m is the weight (g) of MgO_2.

2.3. Characterizations

The crystal structure of the samples were characterized by a X-ray powder diffractometer (XRD, X'Pert Pro) at room temperature with monochromatic Cu K_α radiation (λ = 1.5418 Å). XRD patterns were obtained within the 2θ = 10–90° range and the scanning speed was 2°/min. The infrared spectra of the samples were acquired on a Fourier Transform Infrared Spectrometer (FT-IR, Bruker Vertex 70) in the regular scanning region of 4000–400 cm^{-1}. A field emission transmission electron microscopy (FTEM, Tecnai G2 F30) was used to observe the microstructure and morphology of the samples. The surface morphology of the samples was acquired on a scanning electron microscopy (SEM, Nova NanoSEM 450). The accelerating voltage and the working distance were 10 kV and 5 mm, respectively. A high-performance liquid chromatography-mass spectrometry (HPLC-MS, Agilent 1100 LC/MSD) equipped with an Agilent Eclipse XDB-C18 column (150 × 4.6 mm, 5 μm) was employed to analyze the generated intermediates of RhB degradation in the MgO_2/Fe(III)/TA system. The ESI-MS spectra were acquired in a positive ionization mode with a scan range of m/z 50–800.

2.4. Degradation of organic contaminants

The degradation performance of MgO_2/Fe(III) in the presence of chelating agents was evaluated by degrading RhB in aqueous solution. Specifically, a set amount of chelating agent was added into 100 mL RhB solution (20 mg/L) in a 150 mL glass beaker under constant stirring. Then, 25 mg $Fe_2(SO_4)_3{\cdot}xH_2O$ was added into the above mixture. After all the chemicals thoroughly mixed, 10 mg MgO_2 was added to start the degradation reaction (if not specified, the dosage of MgO_2 was fixed at 10 mg and the molar ratio of MgO_2/Fe(III)/chelating agent was kept at 1 : 0.7 : 0.3). At specific time intervals, 4 mL of solution was taken from the degradation system using a syringe, and filtrated with a 0.22 μm-syringe filter to give filtrate. Afterwards, the concentration of residue RhB in the supernatant was determined on an ultraviolet–visible spectrophotometer (UV-670) and the degradation efficiency of RhB was calculated via Eq. (6). All of the experiments above were conducted in duplicable at 25 °C to ensure the reliability of data.

$$\text{Degradation efficiency } (\%) = \frac{C_0 - C_t}{C_0} \times 100\% \quad (6)$$

Where C_0 and C_t are the initial concentration (mg/L) and remaining concentration (mg/L) at time t of organic contaminants in solution, respectively.

2.5. Electron paramagnetic resonance (EPR) and scavenger tests

The generated ROS in the MgO_2/Fe(III)/TA system was identified by electron paramagnetic resonance (EPR) experiments conducted on a Bruker EMX-micro EPR spectrometer. DMPO was used as a spin-trapping agent to determine ROS generated in the degradation system. At given time interval, 1 mL sample was taken from the MgO_2/Fe(III)/TA system and then 20 μL DMPO was introduced into the extracted sample. After thoroughly mixed, a little mixture was added into a capillary for EPR test. EPR test parameters: the microwave power was 8 mW; the microwave frequency was 9.83 GHz; the modulation frequency was 100 kHz; the constant time was 30 ms; the scanning time was 30 s. To further prove the dominant role of •OH played in organics degradation in the MgO_2/Fe(III)/TA system, the scavenger experiments were carried out. IPA as a common scavenger of •OH was added into the initial RhB solution before degradation.

3. Results and discussion

3.1. Characterizations of MgO_2 nanoparticles

Fig. 1a illustrated the XRD pattern of the obtained MgO_2 sample. Clearly, all diffraction peaks appeared in the XRD pattern could be well indexed to the cubic-structured MgO_2 phase (JCPDS 76–1363). Three typical peaks at $2\theta = 37.1$, 53.5 and 63.7° were ascribed to the (200), (220) and (311) facet of MgO_2, respectively. It was evident that no other peaks related to other compounds such as MgO and $Mg(OH)_2$ were detected, suggesting highly pure MgO_2 product. Furthermore, the active oxygen content ([O]) of as-prepared sample was quantitatively evaluated based on the permanganate titration experiment. The result showed that the [O] achieved 27.2 wt%, near the theoretical active oxygen content (28.6 wt%) of MgO_2. The purity of MgO_2 calculated via Eq. (4) exceeded 95 wt%, further confirming the high purity of MgO_2.

In the FT-IR spectrum of the prepared MgO_2 nanoparticles (Fig. 1b), three peaks appearing at 490 cm^{-1}, 689 cm^{-1} and 866 cm^{-1} resulted from the stretching vibration of Mg–O and O–O bonds, respectively (Wu et al., 2013; Wu et al., 2019). The two absorption peaks at 3429 cm^{-1}, 1510 cm^{-1} were assigned to the asymmetric stretching and bending vibration of the hydroxyl group of adsorbed water (Peng et al., 2017; Wu et al., 2019). The characteristic absorption band at 1429 cm^{-1} corresponded to the vibration of carbonate group originating from the adsorption of CO_2 in air (Jiang et al., 2017; Wu et al., 2019). According to the SEM image of MgO_2 nanoparticles (Fig. 1c), it can be clearly observed that the sample appeared as sheet-like structure, and the nanosheets were composed of nanoparticles with a diameter of around 40 nm. The TEM image (Fig. 1d) indicated that the obtained MgO_2 sample exhibited a fragmented structure containing many nanoparticles, which was in line with the result of SEM.

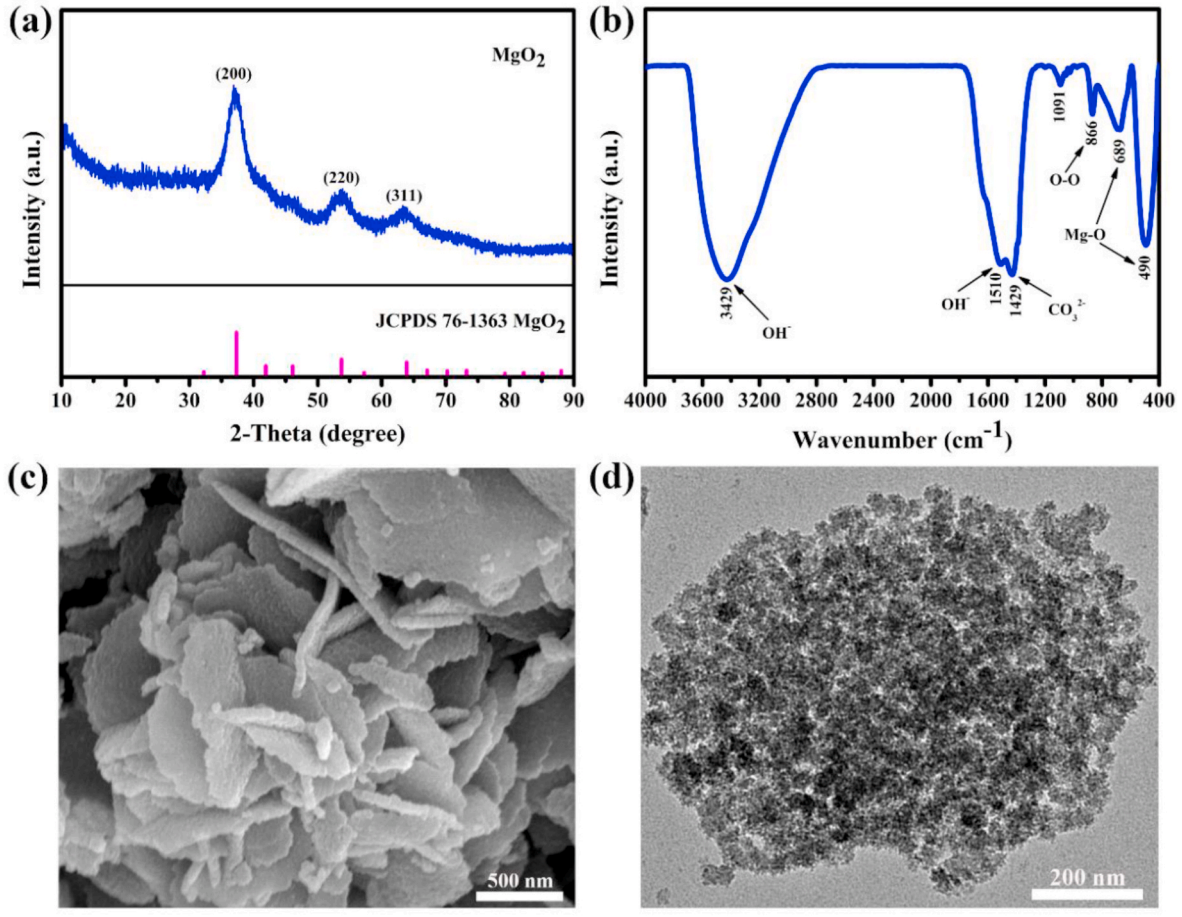

Fig. 1. XRD pattern (a), FT-IR spectrum (b), SEM image (c) and TEM image (d) of MgO_2 nanoparticles.

3.2. Contaminant degradation in the MgO_2/Fe(III)/chelating agent system

3.2.1. Effect of chelating agent

The impact of chelating agents (CA, TA, OA and EDTA) on the performance of MgO_2/Fe(III) system for RhB degradation was evaluated. The molar ratio of chelating agent/MgO_2 was varied from 0 : 1 to 0.5 : 1 and the dosage of $Fe_2(SO_4)_3{\cdot}xH_2O$ was fixed at 25 mg. As illustrated in Fig. 2, the addition of chelating agents can significantly enhance RhB degradation, while RhB removal in the MgO_2/Fe(III) system without any chelating agent was negligible. Within an appropriate dosage range of these four kinds of chelating agents, RhB degradation was enhanced with increasing the dosage of chelating agents. As the molar ratio of CA, TA, OA, and EDTA to MgO_2 is 0.3 : 1, the degradation efficiencies of RhB increased from 6.7% (without any chelating agent) to 42.3%, 98.5%, 48.9% and 25.8% within 30 min, respectively (Fig. S2). While the degradation time was extended to 90 min, the degradation efficiencies of RhB achieved 98.3%, 98.7%, 99.5% and 77.1%, respectively. Evidently, the introduction of these chelating agents could improve RhB degradation to a different extent. The reason that chelating agents boosted the degradation performance of MgO_2/Fe(III) system was related with the increased stability of Fe(III) in aqueous solution. The chelation between chelating agents and Fe(III) can efficiently reduce the formation of ferric precipitate and maintain the concentration of Fe ions in the reaction system, thus efficiently activating MgO_2 to produce ROS (Han et al., 2015; Zhou et al., 2017).

When the molar ratio of CA/MgO_2 was higher than 0.3 : 1 (Fig. 2a), and the molar ratio of TA and EDTA to MgO_2 was higher than 0.4 : 1 (Fig. 2b and d), the degradation rate of RhB began to decline instead. This decline was ascribed to the competition between chelating agents and RhB for ROS to some extent (Liang et al., 2004; Rastogi et al., 2009), since these chelating agents are organics. Moreover, excessive chelating agents would occupy some catalytic sites of Fe(III), thus weakening the catalytic performance of Fe(III). Therefore, RhB degradation could be hindered if excessive chelating agents were added in the MgO_2/Fe(III) system.

To further compare the kinetics of RhB degradation reaction in MgO_2/Fe(III)/chelating agent system (MgO_2: chelating agent = 1 : 0.3), the degradation data of RhB were fitted using pseudo-zero-order, pseudo-first-order and pseudo-second-order kinetic models (Eq. (7)-(9)) (Li et al., 2017; Bao et al., 2017; Cho et al., 2015), respectively.

$$C_0 - C_t = -k_0 \times t \tag{7}$$

$$\ln C_t/C_0 = -k_1 \times t \tag{8}$$

$$\frac{1}{C_t - C_0} = \frac{1}{C_t - C_e} + k_2 \times t \tag{9}$$

Where C_0, C_t, and C_e were the initial concentration (mg/L), concentration (mg/L) at time t and equilibrium concentration (mg/L) of RhB solution, respectively. k_0, k_1 and k_2 were the apparent zero-order kinetic rate constant (mg/L), first-order kinetic rate constant (min^{-1}) and second-order kinetic rate constant (L/mg/min), respectively.

The fitting kinetic curves and corresponding calculated kinetic constants were presented in Fig. 3 and Table S1. Comparing correlation coefficients (R^2), it seemed that the pseudo-zero-order kinetic model was much suitable to manifest RhB degradation in the MgO_2/Fe(III)/OA, MgO_2/Fe(III)/CA and MgO_2/Fe(III)/EDTA systems. While the RhB

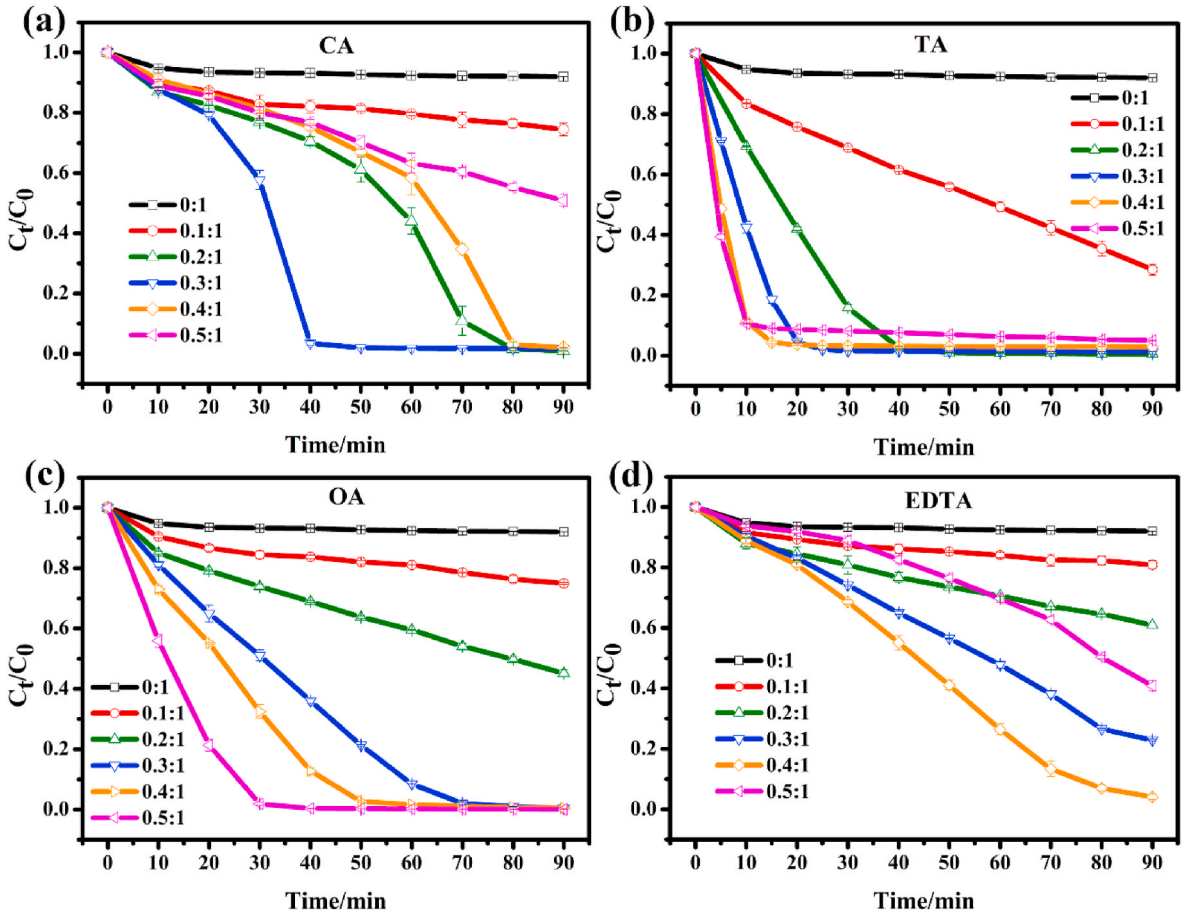

Fig. 2. Influences of CA (a), TA (b), OA (c), EDTA (d) on RhB degradation in the MgO_2/Fe(III) system (Conditions: 100 mL of 20 mg/L RhB solution, 10 mg of MgO_2, 25 mg of $Fe_2(SO_4)_3{\cdot}xH2O$).

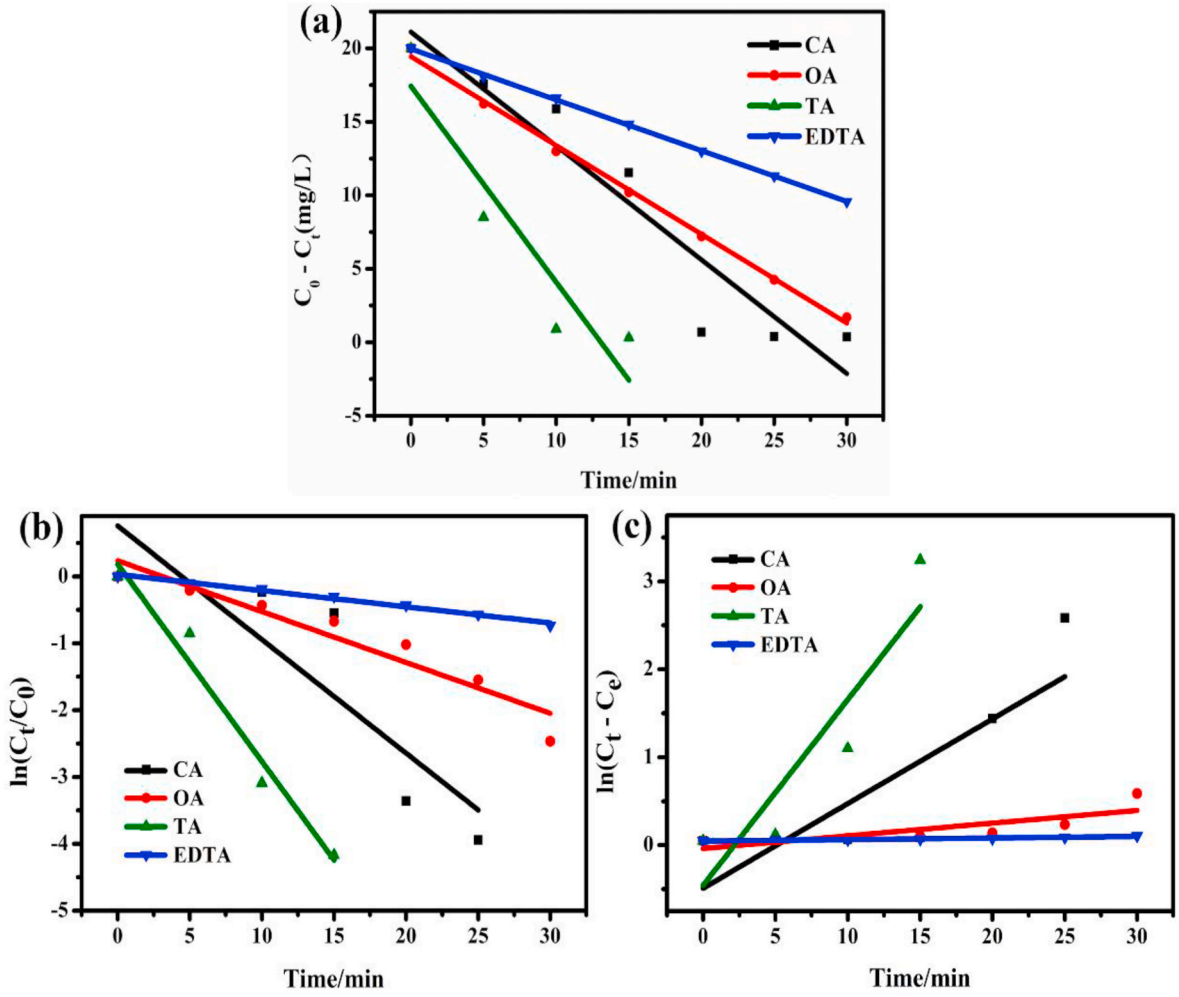

Fig. 3. Pseudo-zero-order kinetic curves (a), pseudo-first-order kinetic curves (b) and pseudo-second-order kinetic curves (c) of RhB degradation in MgO_2/Fe(III)/chelating agent systems.

degradation in MgO_2/Fe(III)/TA system could be well described by the pseudo-first-order kinetic model. The first-order kinetic rate constant of RhB degradation for MgO_2/Fe(III)/TA system reached 0.295 min^{-1}, which is much higher than that with other three chelating agents and in other reported degradation systems (Table 1), indicating that TA possessed a better promoting effect on RhB degradation. The excellent performance of TA might be assigned to the unique molecular structure of TA (Fig. S1), which contained two hydroxyl groups and two carboxyl groups. The characteristic structure of TA would lead to differences in the stability and redox potential of $Fe^{2+}/^{3+}$ chelates with other chelating agents (Zhang et al., 2019c).

3.2.2. *Effect of Fe(III) dosage, temperature, initial solution pH, and other organics degradation*

To inspect the effect of Fe(III) dosages on RhB degradation in the MgO_2/Fe(III)/TA system, a series of experiments were carried out by varying the molar ratio of Fe(III)/MgO_2 from 0.3 : 1 to 0.8 : 1 in the presence of 10 mg MgO_2. As shown in Fig. 4a, the removal efficiency of RhB gradually increased as Fe(III) dosages rose. The RhB removal increased from 83.7% to 98.5% in 30 min with the molar ratio of Fe(III)/MgO_2 increased from 0.3 : 1 to 0.7 : 1. Afterwards, further increasing Fe (III) dosage had no apparent improvement for RhB degradation, indicating that the degradation reaction reached a plateau level when the molar ratio of Fe(III)/MgO_2 reached 0.7 : 1. If without addition of any chelating agents, RhB removal was only 36.9% within 30 min (Fig. S3), even though the molar ratio of Fe(III)/MgO_2 reached up to 2.1 : 1, further confirming the promotion role of chelating agent in the degradation performance of MgO_2/Fe(III) system for organic contaminants.

The performance of MgO_2/Fe(III)/TA system for RhB degradation was examined under different temperatures. From Fig. 4b, it was observed that RhB degradation remarkably enhanced with the rise of temperature. The degradation efficiency of RhB at 5 °C was 81.1% within 60 min. When the temperature was up to 35 °C, the removal efficiency of RhB achieved 98.5% within 15 min, suggesting that the rise of temperature could significantly accelerate RhB removal in MgO_2/Fe (III)/TA system. From the point of molecular dynamics (Huang et al., 2002; Huang and Huang, 2009; Xu and Li, 2010), the average kinetic energy of molecules in the system increased as the temperature rose, and the collision rate between the molecules of the reactants increased, thus accelerating the degradation rate of RhB.

It is well known that the application of conventional Fenton or Fenton-like reactions are seriously limited by the narrow working pH range (2–4). Here, the MgO_2/Fe(III)/TA system was used to degrade RhB solution with different initial pH (3–11). Different from reported Fenton or Fenton-like reactions, the MgO_2/Fe(III)/TA system exhibited exceptional capacity for RhB removal in a wide pH range (3–11) (Fig. 4c). When initial pH was increased from 3 to 11, the degradation efficiencies of RhB slightly reduced from 98.6% to 92.6% within 60 min. Moreover, the degradation rate of RhB in low-pH solution was much fast. At pH = 3 and 5, the degradation efficiencies reached above 95% in 20 min. In this case, a low-pH solution can facilitate the release of H_2O_2 from MgO_2 and further increase the solubility of Fe(III), thus promoting the degradation

Table 1
Comparison of the first-order kinetic rate constants in different systems for RhB degradation.

Degradation system	Volume of RhB solution (mL)	Concentration of RhB (mg/L)	First-order kinetic rate constant (min^{-1})	Reference
MgO_2+Fe(III)+TA	100	20	0.295	This work
MgO_2+Fe(III)+CA	100	20	0.170	This work
MgO_2+Fe(III)+OA	100	20	0.076	This work
MgO_2+Fe(III)+EDTA	100	20	0.024	This work
$LuFeO_3$+ultrasound	20	5	0.032	Zhou et al. (2015)
Fe_3O_4@Polymer@AuNPs + $NaBH_4$	3	10	0.035	Murugan et al. (2015)
ZnO + ultrasound	10	2.5	0.036	Lops et al. (2019)
$CoFe_2O_4$/TNTs + peroxymonosulfate	50	100	0.0628	Du et al. (2016)
$BiVO_4$/Au@CdS + visible light	20	5	0.013	Ye et al. (2018)
H_2O_2+Fe_3O_4	50	5	0.028	Chen et al. (2017)
V_2O_5/g-C_3N_4 +visible light	100	10	0.049	Hong et al. (2016)

performance (Kwon et al., 1999; Thiruvenkatachari et al., 2007). Obviously, the MgO_2/Fe(III)/TA Fenton-like system can be used in both acidic and alkaline solutions. Incidentally, the final pH of corresponding solutions was detected to be 3.5, 4.0, 4.1, 4.4 and 6.3, respectively, which was mainly affected by the acidification of TA and the hydrolyses of Fe(III) and MgO_2.

In addition to RhB, MgO_2/Fe(III)/TA system were also employed to degrade other organic contaminants, and the results were shown in Fig. 4d. The degradation efficiencies of 100 mL MB solution (20 mg/L), TC solution (50 mg/L) and BPA solution (50 mg/L) achieved about 99.1%, 98.6% and 84.4% within 15 min, respectively. Clearly, the MgO_2/Fe(III)/TA system presented excellent degradation performance for these organic contaminants as well.

3.2.3. *Effect of coexisted inorganic anion*

Some inorganic anions existed in wastewater or natural water will consume the produced ROS, inhibiting the degradation capacity of Fenton/Fenton-like reactions (Fu et al., 2015; Zhang et al., 2018a). To explore the impact of coexisted inorganic anions on RhB degradation in the MgO_2/Fe(III)/TA system, four common inorganic anions, NO_3^-, SO_4^{2-}, Cl^- and HCO_3^- with a reasonable concentration gradient were introduced in RhB solution before degradation, respectively.

For NO_3^-, the concentration range of 0–100 mM was used to evaluate its effect on RhB degradation in the MgO_2/Fe(III)/TA system. From Fig. 5a, the addition of NO_3^- in the MgO_2/Fe(III)/TA system had no significant inhibition effect on RhB degradation, similar to previous reports (Chen et al., 2020; López et al., 2013; Zhang et al., 2015). This could be attributed to the fact that the reaction rate of NO_3^- and •OH (Eq.

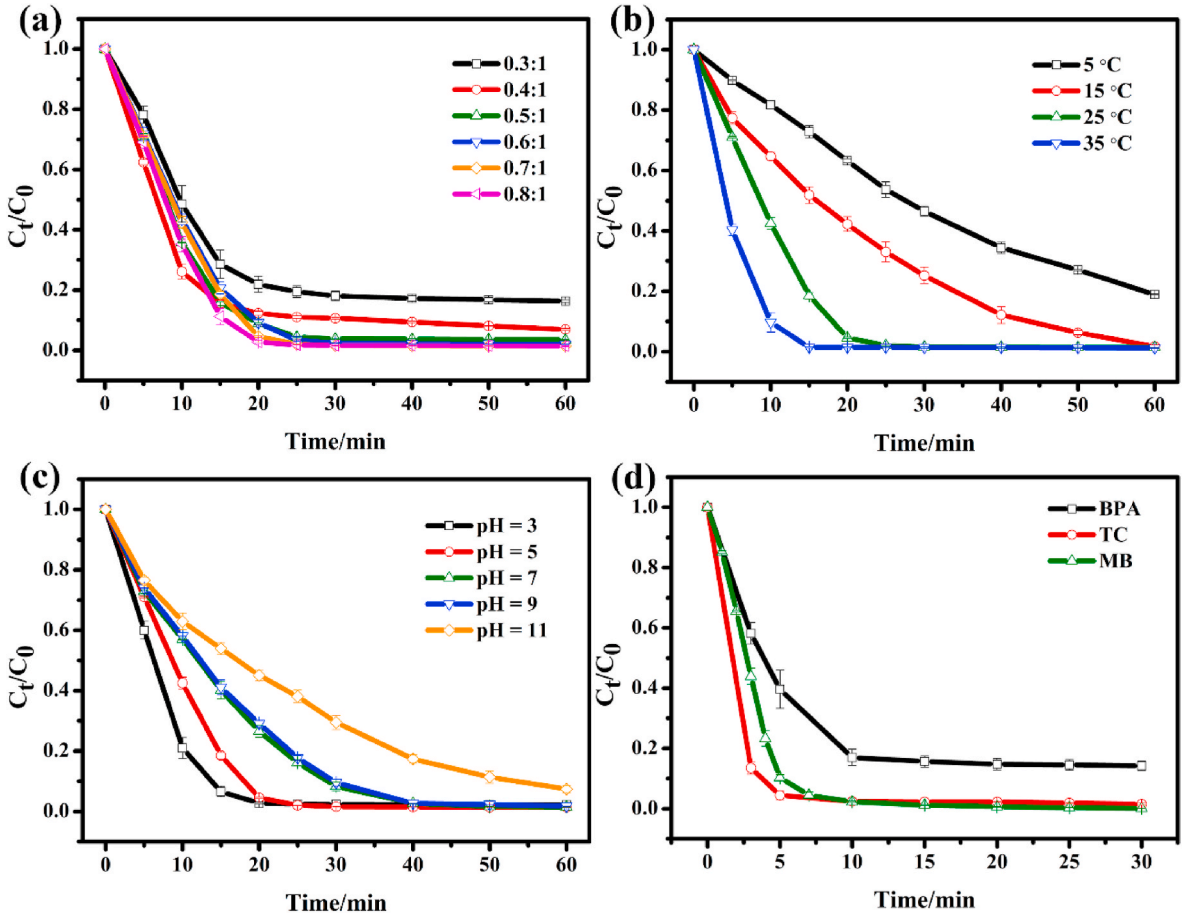

Fig. 4. Influences of the molar ratio of Fe(III) to MgO_2 (a), temperature (b), initial solution pH (c) on RhB degradation and other organics degradation (d) in the MgO_2/Fe(III)/TA system (Conditions: 100 mL of 20 mg/L RhB/50 mg/L BPA/50 mg/L TC/20 mg/L MB solution, 10 mg of MgO_2, 25 mg of $Fe_2(SO_4)_3{\cdot}xH_2O$, and the concentrations of BPA and TC were determined by an Agilent 1260 high performance liquid chromatography).

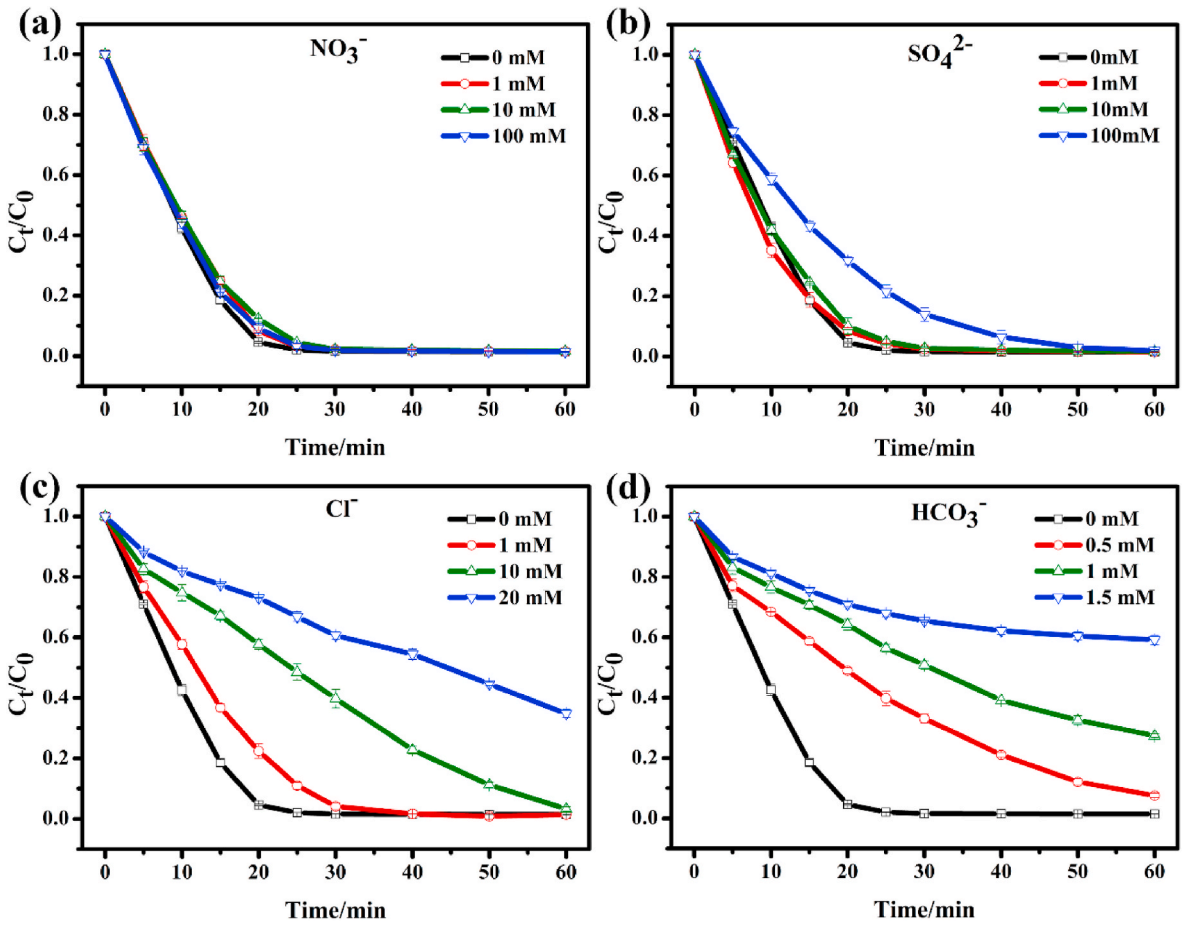

Fig. 5. Influences of different inorganic anions (NO_3^-, SO_4^{2-}, Cl^- and HCO_3^-) on RhB degradation in the MgO_2/Fe(III)/TA system (Conditions: 100 mL of 20 mg/L RhB solution, 10 mg of MgO_2, 25 mg of $Fe_2(SO_4)_3{\cdot}xH_2O$, the molar ratio of TA/MgO_2 at 0.3 : 1).

(10)) is very slow (Guan et al., 2020). Thus, •OH would prefer to react with organic contaminants. As for SO_4^{2-} (Fig. 5b), it almost had no inhibition effect on RhB degradation at the concentrations of 1 mM and 10 mM. However, when the concentration of SO_4^{2-} reached up to 100 mM, SO_4^{2-} exhibited a slight inhibition effect on RhB degradation. The reason of the negative effect was that SO_4^{2-} combined with •OH to form $•SO_4^-$ via Eq. (11), and the generated $•SO_4^-$ had relatively lower oxidation potential than •OH, causing the reduction in degradation rate of RhB (Jo et al., 2016; Khan et al., 2015).

$$NO_3^- + •OH \rightarrow NO_3• + OH^- \quad (10)$$

$$•OH + SO_4^{2-} \rightarrow •SO_4^- + OH^- \quad (11)$$

As illustrated in previous studies (Zhang et al., 2015), Cl^- had a negative influence on the degradation capacities of Fenton or Fenton-like systems. The results of Fig. 5c illustrated that the degradation efficiency of RhB slowly decreased as Cl^- concentration increased. When the Cl^- concentration reached 20 mM, the degradation efficiency was only 65.2% within 60 min. The reason is the fact that Cl^- can combine with •OH to form $•Cl_2^-$ (Eqs. 12–14) (Glaze and Kang, 1989; Trovó et al., 2009), and the activity and oxidation potential of the formed $•Cl_2^-$ was quite lower than those of •OH, leading to a decrease in the degradation efficiency of RhB.

$$Cl^- + •OH \rightarrow •ClOH^- \quad (12)$$

$$•ClOH^- + H^+ \rightarrow •HClOH \quad (13)$$

$$•HClOH + Cl^- \rightarrow •Cl_2^- + H_2O \quad (14)$$

Fig. 5d showed that the degradation efficiency of RhB declined significantly with the rise of HCO_3^- concentration, which is consistent with other reports (Si et al., 2018; Zhang et al., 2018a). When the concentration of HCO_3^- was 1.5 mM, the degradation efficiency of RhB was only 40.9%. The negative effect of HCO_3^- on RhB degradation may be ascribed to the consumption of •OH and H_2O_2 by HCO_3^- (Eq. (15) and Eq. (16)) (Zhang et al., 2015). HCO_3^- can react with •OH to produce $•CO_3^-$, and the generated $•CO_3^-$ can further consume H_2O_2 to produce $•HO_2$ with a low oxidation performance. Therefore, HCO_3^- has a terribly negative effect on the degradation performance of MgO_2/Fe(III)/TA system.

$$HCO_3^- + •OH \rightarrow •CO_3^- + H_2O \quad (15)$$

$$•CO_3^- + H_2O_2 \rightarrow •HO_2 + HCO_3^- \quad (16)$$

In general, the order of influence of these four anions on RhB degradation by the MgO_2/Fe(III)/TA system was $NO_3^- < SO_4^{2-} < Cl^- < HCO_3^-$. Although a certain amount of anions such as Cl^- and HCO_3^- can inhibit the degradation performance, MgO_2/Fe(III)/TA system can still maintain ideal capacity for organics degradation in solutions containing a small amount of inorganic anions, demonstrating that this Fenton-like system has high practicability and broad application prospects in the treatment of groundwater and industrial wastewater.

3.3. Mechanism of organics degradation in the MgO_2/Fe(III)/TA system

The formation of ROS in Fenton or Fenton-like systems is mainly responsible for organics degradation. In order to further determine the main ROS formed in MgO_2/Fe(III)/TA system, EPR experiment was conducted in the presence of DMPO (Fig. 6a). In the spectrum of the

MgO_2/Fe(III)/TA–DMPO mixture, the characteristic fourfold peaks made of a quartet with intensity ratio of 1 : 2 : 2 : 1 and hyperfine coupling of aH = aN = 14.9 G were observed, which were the characteristic signals of the DMPO–•OH adduct (Gao et al., 2018; Cho et al., 2020). On the contrary, no obvious signals related to DMPO–•OH adduct were detected in the EPR spectrum of MgO_2–DMPO mixture, indicating that no •OH generated in the reaction system with MgO_2 alone. The EPR results were consistent with the RhB degradation process in which RhB could be hardly degraded without the addition of Fe(III), suggesting the crucial role of •OH for degrading organic contaminants in the MgO_2/Fe(III)/TA system.

To further prove the significant contribution of •OH in RhB degradation by the MgO_2/Fe(III)/TA system, IPA was added into the degradation system as a scavenger of •OH (Ge et al., 2018; Ma et al., 2015; Zhang et al., 2018b). From Fig. 6b, the degradation efficiency of RhB gradually decreased with the increase of IPA concentration in the degradation system. When the concentration of IPA reached 5 mM, RhB degradation was almost completely suppressed. In addition, p-benzoquinone (BQ) was used as a scavenger to quench superoxide radicals ($\bullet O_2^-$) generated in the MgO_2/Fe(III)/TA system (Fig. S4). It was found that $\bullet O_2^-$ was not critical ROS responsible for RhB degradation in the MgO_2/Fe(III)/TA system. Therefore, the generated •OH was considered to be a dominant role for RhB degradation. Here, the generation of •OH could be described as follows: Firstly, MgO_2 nanoparticles reacted with H_2O to slowly produce H_2O_2 (Fig. S5). Then, the generated H_2O_2 reduced Fe(III) into Fe(II) (Eq. (17)). Finally, H_2O_2 was activated by Fe (II) to yield •OH for RhB degradation, while Fe(II) was oxidized into Fe (III) (Eq. (18)).

$$Fe(III) + H_2O_2 \rightarrow Fe(II) + HO_2\cdot + H^+ \quad (17)$$

$$Fe(II) + H_2O_2 \rightarrow Fe(III) + \bullet OH + OH^- \quad (18)$$

The chelation between TA and Fe(III) was verified through FT-IR technique (Fig. 7a). In comparison with the FT-IR spectrum of TA, the C–OH stretching vibration band of secondary alcohol shifted from 1093 cm^{-1} to 1049 cm^{-1} in the IR spectrum of TA-Fe(III), indicating that Fe (III) might be coordinated with –OH of TA (Palma et al., 2017; Raikwar et al., 2019; Zhao et al., 2016). The disappearance of the broad adsorption peaks between 3300 and 2500 cm^{-1} assigned to HO···H vibration from –COOH confirmed that Fe(III) could also be chelated by –COOH of TA (Hu et al., 2017; Wang et al., 2017). In addition, the characteristic adsorption peaks at 594 cm^{-1} and 480 cm^{-1} revealed the formation of Fe–O bond, further supporting that Fe(III) can interact with –OH or –COOH of TA (Zhang et al., 2019a; Zhang et al., 2019b). To further confirm that the chelation can restrain the precipitation of Fe ions, the concentration of Fe ions in solution was monitored by an atomic absorption spectroscopy (AAS, iCE 3000 series). Fig. 7b showed that the concentration of Fe ions reduced rapidly with the reaction proceeding in the MgO_2/Fe(III) system. After 30 min, almost no Fe was detected in solution. On the contrary, the concentration of Fe ions in the MgO_2/Fe(III)/TA system was basically maintained over 60 mg/L. Therefore, the chelation between TA and Fe(III) efficiently increased the solubility of Fe ions and reduce the formation of ferric precipitate, which would benefit to improve their catalytic performance in Fenton/Fenton-like system.

Since these chelating agents are organic acids, their addition can cause the acidification of the solution, which will also inhibit the precipitation of Fe ions. To investigate the effect of acidification of chelating agents on RhB degradation, a comparison-group experiment was conducted by adjusting the initial pH of RhB solution to the same value of RhB solution in the presence of TA using 0.1 M H_2SO_4 solution. The result (Fig. 7c) showed the degradation efficiency of RhB was only 13.1% within 60 min in the MgO_2/Fe(III)/H_2SO_4 system, far less than that in the MgO_2/Fe(III)/TA system. Evidently, the enhanced degradation ability of the MgO_2/Fe(III)/chelating agent system was dominantly attributed to the chelation between chelating agents and Fe(III), rather than the acidification of chelating agents. According to the above analysis and discussion, the RhB degradation in the MgO_2/Fe(III) and MgO_2/Fe(III)/TA systems was illustrated in Fig. 7d.

3.4. Possible pathway for RhB degradation in the MgO_2/Fe(III)/TA system

To get a further insight into the degradation mechanism of RhB, HPLC-MS technique was used to determine the intermediates generated in the process of RhB degradation. The ESI-MS spectra at different retention time were presented in Fig. S6. The possible pathway of RhB degradation was proposed and illustrated in Fig. 8. The RhB degradation mainly underwent four steps: N-de-ethylation, chromophore structure cleavage, ring-opening and mineralization. As shown in Fig. 8, the mass peaks of m/z 443 and 459 was identified as RhB molecule and the hydroxylated intermediate of RhB (Zhang et al., 2018). The de-ethylation products (m/z 415, 387, 359 and 331) were obtained, due to the droplet of methyl groups from RhB molecule by •OH attack (Zhu et al., 2020; Li et al., 2019). Then, chromophore cleavage occurred between xanthene group and phenyl group, resulting in the generation of intermediates of m/z 318 and 274 (Pang et al., 2020). Subsequently, low-molecular weight acids and alcohols (m/z 122, 110 and 94) were produced by a ring-opening process, and further oxidized into CO_2 and H_2O.

4. Conclusions

In summary, the effect of chelating agents (CA, OA, EDTA, TA) containing different amounts of –COOH and –OH on the degradation

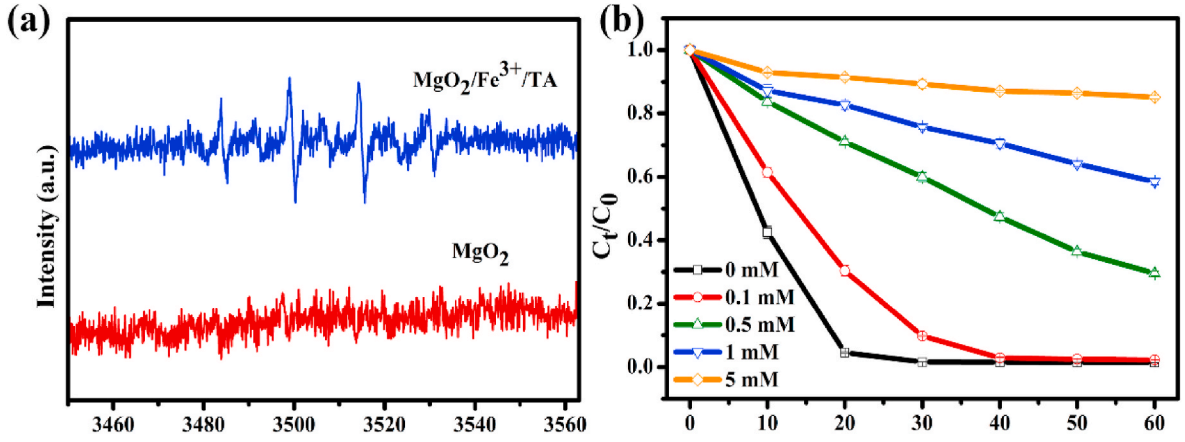

Fig. 6. EPR spectra for detecting DMPO–•OH in MgO_2/Fe(III)/TA and MgO_2 systems (a), RhB degradation in the presence of IPA (b).

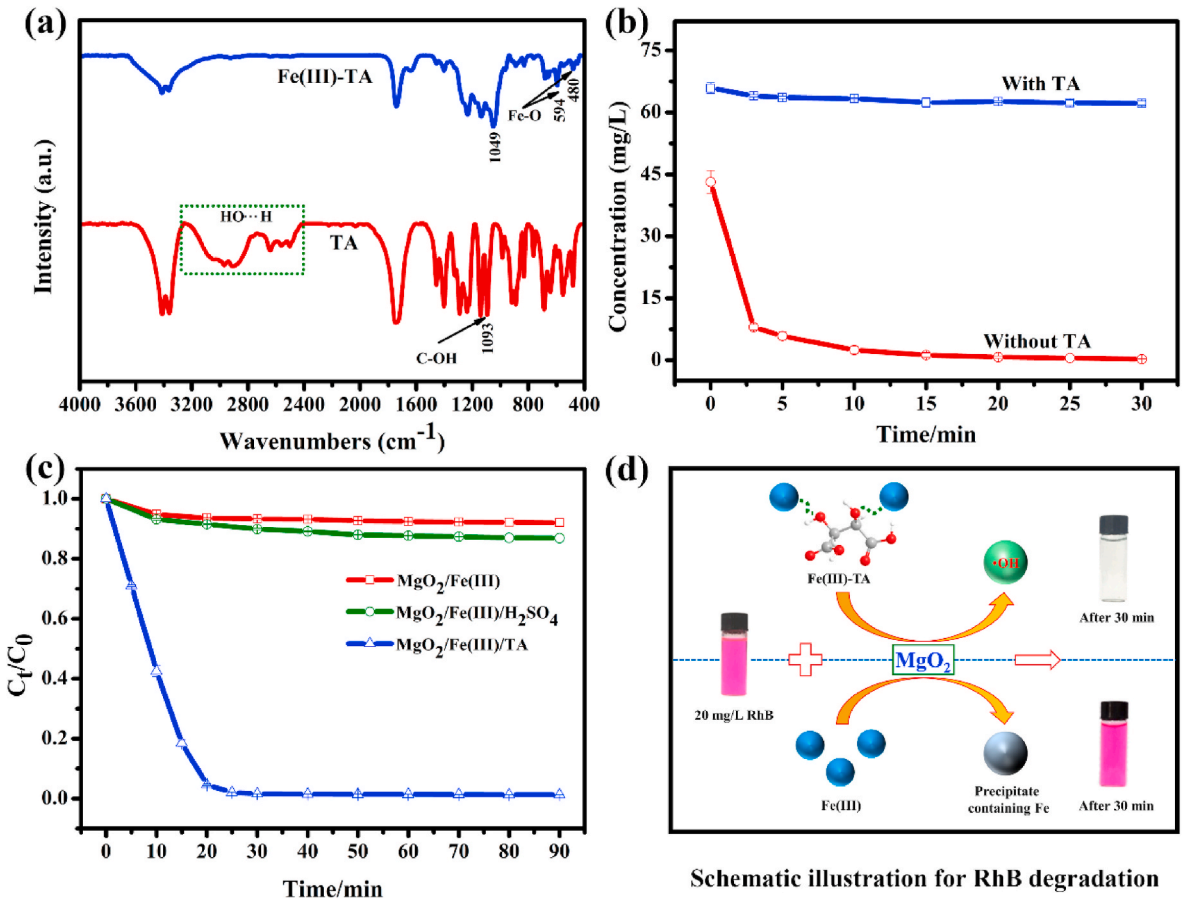

Fig. 7. FT-IR spectra of TA and Fe(III)-TA chelate (a), the concentration of Fe ions in the MgO_2/Fe(III) system with and without TA (b), and RhB degradation in MgO_2/Fe(III)/H_2SO_4, MgO_2/Fe(III) and MgO_2/Fe(III)/TA systems (c), schematic illustration for RhB degradation in the MgO_2/Fe(III) system with and without TA (d).

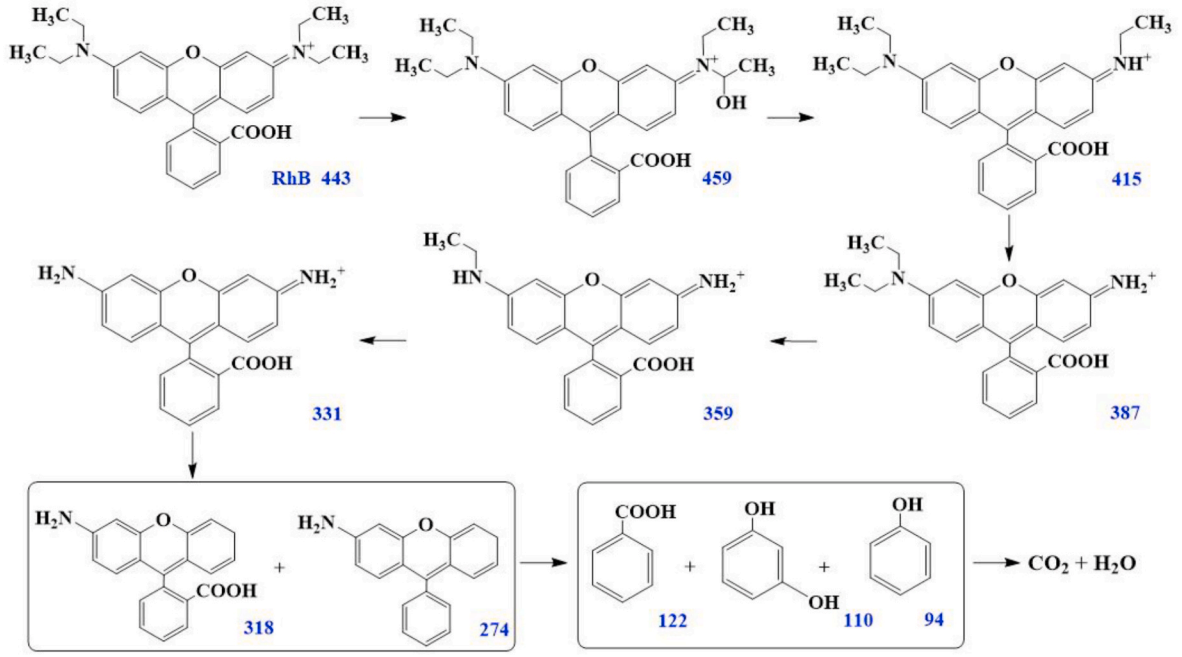

Fig. 8. Possible pathway for RhB degradation in the MgO_2/Fe(III)/TA system.

performance of MgO_2/Fe(III) Fenton-like system was systematically investigated in this work. TA with two –OH and two –COOH exhibited a better promotion effect than other three chelating agents. The degradation efficiency of RhB in the MgO_2/Fe(III)/TA system achieved 98.5% in 30 min. Besides, the MgO_2/Fe(III)/TA system could work in a broad range of pH (3–11) and temperature (5–35 °C). The chelation between TA and Fe(III) was proved to be the key factor for the enhanced degradation performance of MgO_2/Fe(III)/TA system, instead of the acidification of TA. The EPR analysis and scavenger tests indicated that •OH was the dominant ROS, which played a critical role in degrading organic contaminants in the MgO_2/Fe(III)/TA system. Considering the excellent performance, environmental friendliness and a broad range of applications, the MgO_2/Fe(III)/chelating agent Fenton-like system will be an alternative strategy for the treatment of organics-contaminated groundwater and industrial wastewater.

Credit author statement

Yun Bai: Writing - Original Draft, Visualization. Doudou Wu: Methodology, Writing - Review & Editing. Wei Wang: Conceptualization, Investigation, Writing - Review & Editing, Pei Chen: Writing - Review & Editing. Fatang Tan: Validation, Writing - Review & Editing. Xinyun Wang: Funding acquisition, Supervision. Xueliang Qiao: Resources, Supervision. Po Keung Wong: Writing - Review & Editing.

Declaration of competing interest

The authors declare that they have no known competing financial interests or personal relationships that could have appeared to influence the work reported in this paper.

Acknowledgments

The authors acknowledge the experimental help from Huazhong University of Science & Technology Analytical and Testing Center. X. Wang was supported by the National Science Foundation for Distinguished Young Scholars of China (No. 51725504). P.K. Wong was supported by CAS/SAFEA International Partnership Program for Creative Research Teams of Chinese Academy of Sciences (2015HSC-UE004).

Appendix A. Supplementary data

Supplementary data to this article can be found online at https://doi.org/10.1016/j.envres.2020.110242.

References

Bao, Z., Ye, L., Fang, B., Zhao, L., 2017. Synthesis of $Fe_{0.32}Co_{0.68}/\gamma$-$Al_2O_3$@C nanocomposite for depth treatment of dye sewage based on adsorption and advanced catalytic oxidation. J. Mater. Chem. A 5, 6664–6676.

Bararpour, S.T., Feylizadeh, M.R., Delparish, A., Qanbarzadeh, M., Raeiszadeh, M., Feilizadeh, M., 2018. Investigation of 2-nitrophenol solar degradation in the simultaneous presence of $K_2S_2O_8$ and H_2O_2: using experimental design and artificial neural network. J. Clean. Prod. 176, 1154–1162.

Chen, F., Xie, S., Huang, X., Qiu, X., 2017. Ionothermal synthesis of Fe_3O_4 magnetic nanoparticles as efficient heterogeneous Fenton-like catalysts for degradation of organic pollutants with H_2O_2. J. Hazard Mater. 322, 152–162.

Chen, P., Sun, F., Wang, W., Tan, F., Wang, X., Qiao, X., 2020. Facile one-pot fabrication of ZnO_2 particles for the efficient Fenton-like degradation of tetracycline. J. Alloys Compd. 834, 155220.

Cho, K.Y., Yeom, Y.S., Seo, H.Y., Kumar, P., Lee, A.S., Baek, K.Y., et al., 2015. Ionic block copolymer doped reduced graphene oxide supports with ultra-fine Pd nanoparticles: strategic realization of ultra-accelerated nanocatalysis. J. Mater. Chem. A 3, 20471–20476.

Cho, Y., Lin, R., Lin, Y., 2020. Degradation of 2,4-dichlorophenol by CuO-activated peroxydisulfate: importance of surface-bound radicals and reaction kinetics. Sci. Total Environ. 699, 134379.

Du, Y., Ma, W., Liu, P., Zou, B., Ma, J., 2016. Magnetic $CoFe_2O_4$ nanoparticles supported on titanate nanotubes ($CoFe_2O_4$/TNTs) as a novel heterogeneous catalyst for peroxymonosulfate activation and degradation of organic pollutants. J. Hazard Mater. 308, 58–66.

Fu, X., Gu, X., Lu, S., Miao, Z., Xu, M., Zhang, X., et al., 2015. Benzene depletion by Fe (II)-catalyzed sodium percarbonate in aqueous solution. Chem. Eng. J. 267, 25–33.

Gao, H., Yang, H., Xu, J., Zhang, S., Li, J., 2018. Strongly coupled g-C_3N_4 nanosheets-Co_3O_4 quantum dots as 2D/0D heterostructure composite for peroxymonosulfate activation. Small 14, 1801353.

Ge, L., Peng, Z., Wang, W., Tan, F., Wang, X., Su, B., et al., 2018. g-C_3N_4/MgO nanosheets: light-independent, metal-poisoning-free catalysts for the activation of hydrogen peroxide to degrade organics. J. Mater. Chem. A 6, 16421–16429.

Gholami, F., Mosmeri, H., Shavandi, M., Dastgheib, S.M.M., Amoozegar, M.A., 2019. Application of encapsulated magnesium peroxide (MgO_2) nanoparticles in permeable reactive barrier (PRB) for naphthalene and toluene bioremediation from groundwater. Sci. Total Environ. 655, 633–640.

Giannakoudakis, D.A., Florent, M., Wallace, R., Secor, J., Karwacki, C., Bandosz, T.J., 2018. Zinc peroxide nanoparticles: surface, chemical and optical properties and the effect of thermal treatment on the detoxification of mustard gas. Appl. Catal. B Environ. 226, 429–440.

Glaze, W.H., Kang, J.W., 1989. Advanced oxidation processes. Test of a kinetic model for the oxidation of organic compounds with ozone and hydrogen peroxide in a semibatch reactor. Ind. Eng. Chem. Res. 28, 1580–1587.

Guan, C., Jiang, J., Pang, S., Chen, X., Webster, R., Lim, T., 2020. Facile synthesis of pure g-C_3N_4 materials for peroxymonosulfate activation to degrade bisphenol A: effects of precursors and annealing ambience on catalytic oxidation. Chem. Eng. J. 387, 123726.

Han, D., Wan, J., Ma, Y., Wang, Y., Li, Y., Li, D., et al., 2015. New insights into the role of organic chelating agents in Fe(II) activated persulfate processes. Chem. Eng. J. 269, 425–433.

Hong, Y., Jiang, Y., Li, C., Fan, W., Yan, X., Yan, M., et al., 2016. In-situ synthesis of direct solid-state Z-scheme V_2O_5/g-C_3N_4 heterojunctions with enhanced visible light efficiency in photocatalytic degradation of pollutants. Appl. Catal. B Environ. 180, 663–673.

Hu, Q., Zhao, L., Wu, J., Gao, K., Luo, D., Jiang, Y., et al., 2017. In situ dynamic observations of perovskite crystallisation and microstructure evolution intermediated from $[PbI_6]^{4-}$ cage nanoparticles. Nat. Commun. 8, 15688.

Huang, K., Couttenye, R.A., Hoag, G.E., 2002. Kinetics of heat-assisted persulfate oxidation of methyl tert-butyl ether (MTBE). Chemosphere 49, 413–420.

Huang, Y., Huang, Y., 2009. Identification of produced powerful radicals involved in the mineralization of bisphenol A using a novel UV-$Na_2S_2O_8$/H_2O_2-Fe(II, III) two-stage oxidation process. J. Hazard Mater. 162, 1211–1216.

Jiang, X., Li, S., Shao, L., 2017. Pushing CO_2-philic membrane performance to the limit by designing semi-interpenetrating networks (SIPN) for sustainable CO_2 separations. Energy Environ. Sci. 10, 1339–1344.

Jo, E.Y., Lee, T.K., Kim, Y., Park, C.G., 2016. Effect of anions on the removal of bisphenol A in wastewater by electro-oxidation process. Desalin. Water Treat. 57, 29500–29508.

Khan, J.A., Shah, N.S., Khan, H.M., 2015. Decomposition of atrazine by ionizing radiation: kinetics, degradation pathways and influence of radical scavengers. Separ. Purif. Technol. 156, 140–147.

Kwon, B.G., Lee, D.S., Kang, N., Yoon, J., 1999. Characteristics of p-chlorophenol oxidation by Fenton's reagent. Water Res. 33, 2110–2118.

López Peñalver, J.J., Gómez Pacheco, C.V., Sánchez Polo, M., Rivera Utrilla, J., 2013. Degradation of tetracyclines in different water matrices by advanced oxidation/reduction processes based on gamma radiation. J. Chem. Technol. Biotechnol. 88, 1096–1108.

Leal, T.W., Lourenço, L.A., Brandão, H.d.L., da Silva, A., de Souza, S.M.G.U., de Souza, A. A.U., 2018. Low-cost iron-doped catalyst for phenol degradation by heterogeneous Fenton. J. Hazard Mater. 359, 96–103.

Liang, C., Bruell, C.J., Marley, M.C., Sperry, K.L., 2004. Persulfate oxidation for in situ remediation of TCE. II. Activated by chelated ferrous ion. Chemosphere 55, 1225–1233.

Liang, C., Huang, C., Chen, Y., 2008. Potential for activated persulfate degradation of BTEX contamination. Water Res. 42, 4091–4100.

Lops, C., Ancona, A., Di Cesare, K., Dumontel, B., Garino, N., Canavese, G., et al., 2019. Sonophotocatalytic degradation mechanisms of Rhodamine B dye via radicals generation by micro-and nano-particles of ZnO. Appl. Catal. B Environ. 243, 629–640.

Li, X., Wan, T., Qiu, J., Wei, H., Qin, F., Wang, Y., Liao, Y., Huang, Z., Tan, X., 2017. In-situ photocalorimetry-fluorescence spectroscopy studies of RhB photocatalysis over Z-scheme g-C_3N_4@Ag@Ag_3PO_4 nanocomposites: a pseudo-zero-order rather than a first-order process. Appl. Catal. B Environ. 217, 591–602.

Li, J., Yang, F., Zhou, Q., Ren, R., Wu, L., Lv, Y., 2019. A regularly combined magnetic 3D hierarchical Fe_3O_4/BiOBr heterostructure: fabrication, visible-light photocatalytic activity and degradation mechanism. J. Colloid Interface Sci. 546, 139–151.

Liu, J., Yue, Y., Wang, W., Tan, F., Xia, H., Wang, X., Qiao, X., Wong, P.K., 2020a. Facile one-step synthesis of 3D hierarchical flower-like magnesium peroxide for efficient and fast removal of tetracycline from aqueous solution. J. Hazard Mater. 397, 122877.

Liu, J., Yue, Y., Ge, L., Chen, P., Tan, F., Wang, W., Wang, X., Qiao, X., 2020b. Facile fabrication of magnesium peroxide with different morphologies via the isomorphic transformation of magnesium oxide for Fenton-like degradation of methylene blue. Colloid. Surface. A 607, 125499.

Lu, J., Wang, T., Zhou, Y., Cui, C., Ao, Z., Zhou, Y., 2020. Dramatic enhancement effects of L-cysteine on the degradation of sulfadiazine in Fe(III)/CaO_2 system. J. Hazard Mater. 383, 121133.

Ma, B.C., Ghasimi, S., Landfester, K., Vilela, F., Zhan, g K.A., 2015. Conjugated microporous polymer nanoparticles with enhanced dispersibility and water compatibility for photocatalytic applications. J. Mater. Chem. A 3, 16064–16071.

Miao, W., Liu, Y., Chen, X., Zhao, Y., Mao, S., 2020. Tuning layered Fe-doped g-C_3N_4 structure through pyrolysis for enhanced Fenton and photo-Fenton activities. Carbon 159, 461–470.
Miao, Z., Gu, X., Lu, S., Brusseau, M.L., Zhang, X., Fu, X., et al., 2015. Enhancement effects of chelating agents on the degradation of tetrachloroethene in Fe(III) catalyzed percarbonate system. Chem. Eng. J. 281, 286–294.
Miklos, D.B., Remy, C., Jekel, M., Linden, K.G., Drewes, J.E., Huebner, U., 2018. Evaluation of advanced oxidation processes for water and wastewater treatment–a critical review. Water Res. 139, 118–131.
Moreira, F.C., Boaventura, R.A., Brillas, E., Vilar, V.J., 2017. Electrochemical advanced oxidation processes: a review on their application to synthetic and real wastewaters. Appl. Catal. B Environ. 202, 217–261.
Murugan, E., Jebaranjitham, J.N., 2015. Dendrimer grafted core–shell Fe_3O_4–polymer magnetic nanocomposites stabilized with AuNPs for enhanced catalytic degradation of Rhodamine B–A kinetic study. Chem. Eng. J. 259, 266–276.
Northup, A., Cassidy, D., 2008. Calcium peroxide (CaO_2) for use in modified Fenton chemistry. J. Hazard Mater. 152, 1164–1170.
Ouyang, Q., Kou, F., Tsang, P.E., Lian, J., Xian, J., Fang, J., et al., 2019a. Green synthesis of Fe-based material using tea polyphenols and its application as a heterogeneous Fenton-like catalyst for the degradation of lincomycin. J. Clean. Prod. 232, 1492–1498.
Ouyang, Q., Kou, F., Zhang, N., Lian, J., Tu, G., Fang, Z., 2019b. Tea polyphenols promote Fenton-like reaction: pH self-driving chelation and reduction mechanism. Chem. Eng. J. 366, 514–522.
Palma, L.M., Almeida, T.S., Morais, C., Napporn, T.W., Kokoh, K.B., de Andrade, A.R., 2017. Effect of Co-catalyst on the selective electrooxidation of glycerol over Ruthenium-based nanomaterials. ChemElectroChem 4, 39–45.
Pang, Y., Kong, L., Chen, D., Yuvaraja, G., Mehmood, S., 2020. Facilely synthesized cobalt doped hydroxyapatite as hydroxyl promoted peroxymonosulfate activator for degradation of Rhodamine B. J. Hazard Mater. 384, 121447.
Peng, Z., Xiong, C., Wang, W., Tan, F., Xu, Y., Wang, X., et al., 2017. Facile modification of nanoscale zero-valent iron with high stability for Cr(VI) remediation. Sci. Total Environ. 596, 266–273.
Pignatello, J.J., Oliveros, E., MacKay, A., 2006. Advanced oxidation processes for organic contaminant destruction based on the Fenton reaction and related chemistry. Crit. Rev. Environ. Sci. Technol. 36, 1–84.
Pulgarin, A., Giannakis, S., Pulgarin, C., Ludwig, C., Refardt, D., 2020. A novel proposition for a citrate-modified photo-Fenton process against bacterial contamination of microalgae cultures. Appl. Catal. B Environ. 265, 118615.
Qin, Y., Song, F., Ai, Z., Zhang, P., Zhang, L., 2015. Protocatechuic acid promoted alachlor degradation in Fe(III)/H_2O_2 Fenton system. Environ. Sci. Technol. 49, 7948–7956.
Raikwar, D., Majumdar, S., Shee, D., 2019. Thermocatalytic depolymerization of Kraft lignin to guaiacols using HZSM-5 in alkaline water-THF co-solvent: a realistic approach. Green Chem. 21, 3864–3881.
Rastogi, A., Al-Abed, S.R., Dionysiou, D.D., 2009. Effect of inorganic, synthetic and naturally occurring chelating agents on Fe(II) mediated advanced oxidation of chlorophenols. Water Res. 43, 684–694.
Si, X., Wu, K., Si, Y., Yousaf, B., 2018. Synergistic effects and mechanisms of hydroxyl radical-mediated oxidative degradation of sulfamethoxazole by Fe(II)-EDTA catalyzed calcium peroxide: implications for remediation of antibiotic-contaminated water. Chem. Eng. J. 353, 80–91.
Subramanian, G., Madras, G., 2017. Remarkable enhancement of Fenton degradation at a wide pH range promoted by thioglycolic acid. Chem. Commun. 53, 1136–1139.
Sun, F., Liu, H., Wang, H., Shu, D., Chen, T., Zou, X., Huang, F., 2020. A novel discovery of a heterogeneous Fenton-like system based on natural siderite: a wide range of pH values from 3 to 9. Sci. Total Environ. 699, 134293.
Thiruvenkatachari, R., Kwon, T.O., Jun, J.C., Balaji, S., Matheswaran, M., Moon, I.S., 2007. Application of several advanced oxidation processes for the destruction of terephthalic acid (TPA). J. Hazard Mater. 142, 308–314.
Trovó, A.G., Nogueira, R.F., Agüera, A., Sirtori, C., Fernández-Alba, A.R., 2009. Photodegradation of sulfamethoxazole in various aqueous media: persistence, toxicity and photoproducts assessment. Chemosphere 77, 1292–1298.
Wang, J., Wang, S., 2018. Activation of persulfate (PS) and peroxymonosulfate (PMS) and application for the degradation of emerging contaminants. Chem. Eng. J. 334, 1502–1517.
Wang, Y., Qu, Q., Liu, G., Battaglia, V.S., Zheng, H., 2017. Aluminum fumarate-based metal organic frameworks with tremella-like structure as ultrafast and stable anode for lithium-ion batteries. Nanomater. Energy 39, 200–210.
Wolanov, Y., Prikhodchenko, P.V., Medvedev, A.G., Pedahzur, R., Lev, O., 2013. Zinc dioxide nanoparticulates: a hydrogen peroxide source at moderate pH. Environ. Sci. Technol. 47, 8769–8774.
Wu, D., Bai, Y., Wang, W., Xia, H., Tan, F., Zhang, S., et al., 2019. Highly pure MgO_2 nanoparticles as robust solid oxidant for enhanced Fenton-like degradation of organic contaminants. J. Hazard Mater. 374, 319–328.
Wu, X., Tan, X., Yang, S., Wen, T., Guo, H., Wang, X., et al., 2013. Coexistence of adsorption and coagulation processes of both arsenate and NOM from contaminated groundwater by nanocrystallined Mg/Al layered double hydroxides. Water Res. 47, 4159–4168.
Xu, X., Li, X., 2010. Degradation of azo dye Orange G in aqueous solutions by persulfate with ferrous ion. Separ. Purif. Technol. 72, 105–111.
Xue, Y., Lu, S., Fu, X., Sharma, V.K., Mendoza-Sanchez, I., Qiu, Z., et al., 2018. Simultaneous removal of benzene, toluene, ethylbenzene and xylene (BTEX) by CaO_2 based Fenton system: enhanced degradation by chelating agents. Chem. Eng. J. 331, 255–264.
Yamaguchi, R., Kurosu, S., Suzuki, M., Kawase, Y., 2018. Hydroxyl radical generation by zero-valent iron/Cu (ZVI/Cu) bimetallic catalyst in wastewater treatment: heterogeneous Fenton/Fenton-like reactions by Fenton reagents formed in-situ under oxic conditions. Chem. Eng. J. 334, 1537–1549.
Ye, F., Li, H., Yu, H., Chen, S., Quan, X., 2018. Constructing $BiVO_4$-Au@CdS photocatalyst with energic charge-carrier-separation capacity derived from facet induction and Z-scheme bridge for degradation of organic pollutants. Appl. Catal. B Environ. 227, 258–265.
Yu, S., Gu, X., Lu, S., Xue, Y., Zhang, X., Xu, M., et al., 2018. Degradation of phenanthrene in aqueous solution by a persulfate/percarbonate system activated with CA chelated-Fe(II). Chem. Eng. J. 333, 122–131.
Yue, Y., Zhang, P., Wang, W., Cai, Y., Tan, F., Wang, X., Qiao, X., Wong, P., 2020. Enhanced dark adsorption and visible-light-driven photocatalytic properties of narrower-band-gap Cu_2S decorated Cu_2O nanocomposites for efficient removal of organic pollutants. J. Hazard Mater. 384, 121302.
Zhang, A., Shen, X., Yin, X., Li, X., Liu, Y., 2018a. Application of calcium peroxide for efficient removal of triamcinolone acetonide from aqueous solutions: mechanisms and products. Chem. Eng. J. 345, 594–603.
Zhang, C., Liu, S., Chen, T., Li, Z., Hao, J., 2019a. Oxygen vacancy-engineered Fe_2O_3 nanocubes via a task-specific ionic liquid for electrocatalytic N_2 fixation. Chem. Commun. 55, 7370–7373.
Zhang, P., Hou, Y., Zeng, J., Li, Y., Wang, Z., Zhu, R., et al., 2019b. Coordinatively unsaturated Fe(III) based activable probes for enhanced MRI and therapy of tumors. Angew. Chem. Int. Ed. https://doi.org/10.1002/anie.201904880.
Zhang, Q., Chen, P., Zhuo, M., Wang, F., Su, Y., Chen, T., et al., 2018b. Degradation of indometacin by simulated sunlight activated CDs-loaded $BiPO_4$ photocatalyst: roles of oxidative species. Appl. Catal. B Environ. 221, 129–139.
Zhang, X., Gu, X., Lu, S., Miao, Z., Xu, M., Fu, X., et al., 2015. Degradation of trichloroethylene in aqueous solution by calcium peroxide activated with ferrous ion. J. Hazard Mater. 284, 253–260.
Zhang, Y., Zhou, J., Cai, W., Zhou, J., Li, Z., 2018c. Enhanced photocatalytic performance and degradation pathway of Rhodamine B over hierarchical double-shelled zinc nickel oxide hollow sphere heterojunction. Appl. Surf. Sci. 430, 549–560.
Zhao, P., Zhang, J., Li, Q., Wang, C., 2016. Electrochemical performance of fulvic acid-based electrospun hard carbon nanofibers as promising anodes for sodium-ion batteries. J. Power Sources 334, 170–178.
Zhou, M., Yang, H., Xian, T., Li, R., Zhang, H., Wang, X., 2015. Sonocatalytic degradation of RhB over $LuFeO_3$ particles under ultrasonic irradiation. J. Hazard Mater. 289, 149–157.
Zhou, Y., Fang, X., Wang, T., Hu, Y., Lu, J., 2017. Chelating agents enhanced CaO_2 oxidation of bisphenol A catalyzed by Fe(III) and reuse of ferric sludge as a source of catalyst. Chem. Eng. J. 313, 638–645.
Zhu, K., Bin, Q., Shen, Y., Huang, J., He, D., Chen, W., 2020. In-situ formed N-doped bamboo-like carbon nanotubes encapsulated with Fe nanoparticles supported by biochar as highly efficient catalyst for activation of persulfate (PS) toward degradation of organic pollutants. Chem. Eng. J. 402, 126090.